



The composition and compression of biofilms developed on ultrafiltration membranes determine hydraulic biofilm resistance

Nicolas Derlon ^{a, b,*}, Alexander Grüter ^a, Fabienne Brandenberger ^a, Anja Sutter ^a, Ute Kuhlicke ^c, Thomas R. Neu ^c, Eberhard Morgenroth ^{a, b}

^a Eawag, Swiss Federal Institute of Aquatic Science and Technology, Department of Process Engineering, CH-8600 Dübendorf, Switzerland

^b ETH Zürich, Institute of Environmental Engineering, CH-8093 Zürich, Switzerland

^c Helmholtz Centre for Environmental Research – UFZ, Magdeburg, Germany



ARTICLE INFO

Article history:

Received 11 April 2016

Received in revised form

6 June 2016

Accepted 8 June 2016

Available online 9 June 2016

Keywords:

Biofilm

Permeability

Hydraulic resistance

Compression

Extracellular polymeric substances (EPS)

Ultrafiltration membrane

ABSTRACT

This study aimed at identifying how to improve the level of permeate flux stabilisation during gravity-driven membrane filtration without control of biofilm formation. The focus was therefore on understanding (i) how the different fractions of the biofilms (inorganics particles, bacterial cells, EPS matrix) influence its hydraulic resistance and (ii) how the compression of biofilms impacts its hydraulic resistance, i.e., can water head be increased to increase the level of permeate flux stabilisation. Biofilms were developed on ultrafiltration membranes at 88 and 284 cm water heads with dead-end filtration for around 50 days. A larger water head resulted in a smaller biofilm permeability (150 and 50 L m⁻² h⁻¹ bar⁻¹ for biofilms grown at 88 cm and 284 cm water head, respectively). Biofilms were mainly composed of EPS (>90% in volume). The comparison of the hydraulic resistances of biofilms to model fouling layers indicated that most of the hydraulic resistance is due to the EPS matrix. The compressibility of the biofilm was also evaluated by subjecting the biofilms to short-term (few minutes) and long-term variations of transmembrane pressures (TMP). A sudden change of TMP resulted in an instantaneous and reversible change of biofilm hydraulic resistance. A long-term change of TMP induced a slow change in the biofilm hydraulic resistance. Our results demonstrate that the response of biofilms to a TMP change has two components: an immediate variation of resistance (due to compression/relaxation) and a long-term response (linked to biofilm adaptation/growth). Our results provide relevant information about the relationship between the operating conditions in terms of TMP, the biofilm structure and composition and the resulting biofilm hydraulic resistance. These findings have practical implications for a broad range of membrane systems.

© 2016 Elsevier Ltd. All rights reserved.

1. Introduction

Biofilms inevitably grow on membrane surfaces and reduce permeate flux. So far the operation of membrane systems mainly relied on avoiding biofilm formation. Different strategies were developed to control the biofilm growth. But recent studies suggested that it might be possible or desirable to live with biofilm (Derlon et al., 2014; Dreszer et al., 2013). Biofilm-membrane composite system indeed have multiple advantages compared to membrane system only – flux stabilisation, improved permeate

quality. Whatever the selected approach (living with or fighting the biofilms), it is key to understand what factors determine the hydraulic resistance of biofilms. This is especially relevant for membrane systems where biofilm formation is fully tolerated (Derlon et al., submitted) or controlled to a low extent (Smith et al., 2015).

Biofilms are dynamic and complex structures made of different organic (e.g., cells, EPS) and inorganic fractions. Mass transport of soluble substrates and fluid dynamic outside of the biofilm is rather well understood. But very little information about the water flow through the biofilm itself is available. Convection through biofilms has been studied for biofilms developed on solid substrata under cross-flow conditions (de Beer et al., 1996; Lewandowski et al., 1995; Stoodley et al., 1994). Convection around and sometimes through cell clusters was observed using fluorescein or fluorescent particles (de Beer et al., 1994; Stoodley et al., 1994) (Fig. 1a). A

* Corresponding author. Eawag, Swiss Federal Institute of Aquatic Science and Technology, Department of Process Engineering, CH-8600 Dübendorf, Switzerland.
E-mail address: Nicolas.derlon@eawag.ch (N. Derlon).

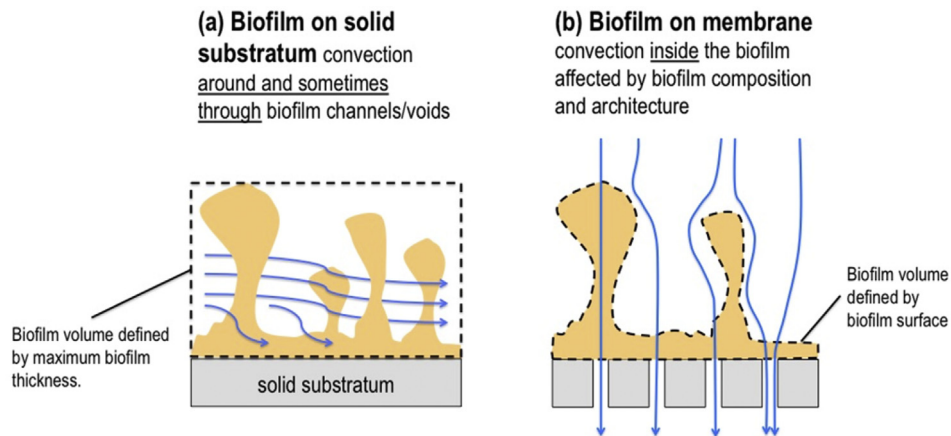


Fig. 1. Conceptual representations of convection through (a) Conceptual representation of convection through biofilms grown on solid substrata. The flow occurs here mainly between the biofilm heterogeneities and sometimes beads penetrate the biofilm matrix. (b) Conceptual representation of convection through biofilms grown on permeable substrata such as membranes, i.e., the main research question addressed in this study.

similar observation was reported for heterogeneous biofilms developed in porous media, for which advection is often observed around heterogeneities (Flemming et al., 2000). These studies were then extensively cited and it became well accepted that convection occurs inside the biofilms. However, channels in the studies of Stoodley et al. (1994) and de Beer et al. (1994) refer to external voids, i.e., to the valleys or conduits separating cells clusters, streamers or other structural heterogeneities. Thus, it still remains unclear whether convection occurs inside the volume of the biofilms that is defined by the biofilm-bulk interface vs. convection inside the volume defined by the maximum biofilm thickness as observed in the studies of Stoodley et al. (1994).

Understanding what are the factors that influence the hydraulic resistance of biofilms is particularly important for membrane biofilms (Fig. 1b). It is especially important to identify how the composition and internal architecture of the biofilms may influence permeation (e.g., presence of internal voids/channels, cells, EPS matrix) (Fig. 1b). The comparison of the hydraulic resistances of biofilms with the one of model fouling layers gave initial insights about the relationship between composition and hydraulic resistance. Different studies suggested that EPS might be the main contributor to biofilm hydraulic resistance (Dreszer et al., 2013; Mcdonogh et al., 1994; Stewart, 2012). Stewart (2012) compared the permeability of model fouling layers made of spheres or hydrated gels. The layers made of spheres were more permeable than the layers of hydrated gels. Stewart (2012) thus concluded that the EPS content of biofilms governs the biofilm permeability. Dreszer et al. (2013) compared the overall resistances of bacterial cell layer and biofilms (containing the same amount of cells). The overall resistance of the cell layer was significantly smaller than the overall resistance of a biofilm that contained the same volume of cells (6-fold difference). Dreszer et al. (2013) thus attributed the difference in the hydraulic resistances to the EPS. However the mass/thickness of the cell layer was much lower than those of the biofilm. The difference between the specific resistances (resistance relative to mass or thickness) is less pronounced than the one of the absolute resistances (3-fold vs. 6-fold, respectively). The work of Stewart (2012) and Dreszer et al. (2014) thus provide plausible insights about the influence of the EPS on the biofilm permeability. But other studies reported contradictory findings, i.e., that bacterial cells are more resistant to permeation than EPS (Mcdonogh et al., 1994). Thus, it is still required to evaluate how the different biofilm fractions (inorganic particles, cells and EPS) impact its hydraulic resistance.

Better understanding how biofilm mechanics (e.g., compression) influence the biofilm permeability is also an important aspect of membrane biofilms. It is intuitive that the biofilm composition likely determines the mechanical properties of the biofilms, i.e., how biofilms respond to stresses and ultimately change their internal structure and permeability. Biofilms grown on solid substrata under cross-flow conditions behave as viscoelastic material (Stoodley et al., 1999a, 1999b). The strain increases linearly at low load (elastic response) and then a creep is observed over time (viscoelastic response). Studies that applied a normal force also showed that biofilms are compressible. Pure culture biofilms from the dental pathogen *Streptococcus mutans* were for example highly compressible when applying a normal force of 0.1 N over a 25 mm diameter disk (Vinogradov et al., 2006). However, very little is known about the compressibility of biofilms growing on permeable substrata such as membranes. Young biofilms grown on membrane surfaces with acetate-based feed solutions were shown to be compressible when increasing the permeate flux from 20 to 60 L m⁻² h⁻¹ (Dreszer et al., 2014). The study of Dreszer et al. (2014) delivered very relevant insights about the effect of an increased TMP on biofilm compressibility and resistance. But the compressibility of biofilms must also be evaluated for older biofilms characterised by a more complex composition.

This study aims at better understanding (i) how the biofilm composition (inorganic fraction, cells, EPS) influences its hydraulic resistance and (ii) how the mechanical properties of the biofilms (compressibility) ultimately influences its hydraulic resistance. Biofilms were developed during gravity-driven membrane ultrafiltration at two different water heads: 88 and 284 cm. Permeate flux and permeability were analysed with regard of the biofilm composition. Biofilm composition was characterised in terms of inorganic and organic carbon (bacterial cells, EPS) concentrations and volumes. Biofilms of different ages were then submitted to short- and long-term step-wise increase of TMP and to evaluate their compressibility.

2. Materials and methods

2.1. Operating conditions

Two types of experiments were performed in this study: (1) long-term filtration experiments with biofilm formation on membrane surfaces at a constant pressure for several weeks (Exp. 1.1, Table 1 first row) or at constant pressure during an initial growth

Table 1

Details of the different experiments performed: (1) long-term experiments at constant (Exp. 1.1) or switched water heads (Exp. 1.2) and (2) short-terms experiment with step-wise increase of the TMP (Exp. 2).

| Experiment | TMP (bar) | Experimental system | Measured variables |
|---|--|--|---|
| (1) Long-term filtration experiments | (1.1) Long-term application (50 d) of a constant water head of 88 or 284 cm | Biofilms developed during GDM filtration | <ul style="list-style-type: none"> • Flux, resistances, permeability • Biofilm physical structure • Mesoscale structure using Optical Coherence Tomography • Microscale structure using lectin-staining and Confocal Laser Scanning Microscopy • Biofilm composition • Total organic and inorganic carbon content • EPS and bacterial cell volumes • Short-term and long-term changes in the flux, resistances and permeability |
| (2) Short term filtration experiments with model fouling layers or biofilms | (1.2) Long-term application of a constant water head of 88 cm, then switch to 284 cm, and vice-versa. Initial water heads applied for 6, 16, 22, 25, 35, or 49 days. Short-term application of a step-wise TMP increase: 0.2, 0.8, 1.5 and 2.5 bar for 2 min. Second step-wise TMP increase applied after 4 min of relaxation. | Biofilms developed during GDM filtration <ul style="list-style-type: none"> • Biofilms developed during GDM filtration • Model cake layers (4 g m^{-2}): • Kaolin • Diatoms • Bacterial cells • Activated sludge flocs • Aerobic granules | <ul style="list-style-type: none"> • Change in flux, resistances, permeability with the step-wise increase of TMP |

period and then switch to another TMP for several days/weeks (Exp. 1.2, *Table 1* second row), and (2) short-term experiments with step-wise increase of the TMP (Exp. 2, *Table 1* third row). In exp. 1.1 the biofilms were grown over long-term (50 days) at constant water heads of 88 cm or 284 cm. Exp. 1.1 was repeated twice (run 1 and 2). In exp. 1.2 the biofilms were grown during 6, 16, 22, 25, 35 or 49 days at an initial water head of 88 cm and then exposed to 284 cm, and vice-versa. The second TMP was also applied for several days/weeks. In exp. 2 biofilms of different ages and model fouling layers were exposed to step-wise increases of the TMP. TMPs of 0.2, 0.8, 1.5 and 2.5 bar were applied for 2 min (*Figure SI-1*). Two cycles of step-wise TMP increase were applied (4 min relaxation in between). For all experiments, the filtration performances (permeate flux, resistances and permeability) were monitored. For experiment 1.1 the biofilm physical and biochemical structures were also characterised.

2.2. Experimental set-up

2.2.1. GDM set-up for long-term filtration experiment (exp. 1.1 and 1.2)

Biofilms were grown in gravity-driven ultrafiltration systems at two different water heads: 88 cm and 284 cm. Five parallel biofilms were grown under each condition in terms of water head. The GDM systems were operated in dead-end mode without control of the biofilm formation (i.e., no chemical cleaning, no back-washing, etc.) for around 50 days. The GDM systems consisted of water tanks connected to five biofouling monitors (for each condition) using silicon tubing. The water tanks were equipped with an over-flow to maintain constant water heads. Raw water from a creek (Chriesbach, Dübendorf, Switzerland) was continuously fed at the bottom of the water tank. The detailed characteristics (Total organic carbon, assimilable organic carbon, etc.) of the Chriesbach creek water can be found in [Derlon et al. \(2013\)](#). Water and room temperatures were controlled at 20 °C. The Hydraulic Retention Time (HRT) was

controlled to around 4 h in each water tank.

2.2.2. Experimental set-up for short-term experiment (exp. 2)

Biofilms and model fouling layers were developed in 400 mL non-stirred Amicon cells (Merck Millipore, Schaffhausen, Switzerland). Fouling layers made of different inorganic or organic compounds were prepared at equal concentration of 4 g m^{-2} . This concentration was chosen according to previous measurements of biofilm mass ([Derlon et al., 2012](#)). The different inorganic and organic compounds tested in this study were: kaolin (Fluka, 60609), diatoms (Fluka, 60779), bacterial cells, activated sludge flocs, aerobic granules. Bacterial cells culture were grown using Evian water as inoculum and medium. Acetate was used as carbon source. Activated sludge flocs and aerobic granules were sampled from wastewater treatment plants that treat municipal wastewater (Eawag, Dübendorf, Switzerland).

2.2.3. Membrane and biofouling monitors

Polyethersulfone membranes (UP150, Microdyn Nadir, Wiesbaden, Germany) with a nominal cut-off of 150 kDa were used in this study. The membrane surface was 0.00231 m^2 . Virgin membranes were cleaned for 24 h in deionized water to remove chemical agents. The

deionized water was renewed several times during this period. More information about the biofouling monitors can be found in [Derlon et al. \(2014\)](#).

2.3. Biofilm characterization

2.3.1. Physical structure at mesoscale (optical coherence tomography)

Optical coherence tomography (OCT) (model 930 nm Spectral Domain, Thorlabs GmbH, Dachau, Germany) was used to investigate the mesoscale structure of the biofilms (exp. 1.1). The use of long wavelength light allows penetrating up to a depth of 2.7 mm

(in air, i.e., with a refractive index of 1) with axial and lateral resolutions of 4.4 µm and 15 µm, respectively. For biofilms penetration depths up to 1.7 mm are usually observed due to the higher refractive index. Around 20 images of biofilm cross sections (width x high: 2 × 1 mm) were acquired at different time intervals for each filtration module. Imaging was performed at atmospheric pressure (i.e., without TMP) for the 5 flow-cells of each condition. Around 20 measurements were performed per flow cells. Image analysis software implemented in Matlab® (MathWorks, Natick, US) was used to quantify the biofilm physical structure (mean biofilm thickness, absolute and relative biofilm roughness). Details about the calculations can be found in Derlon et al. (2012). Standard deviations were calculated for the entire set of measurements (i.e., 20 measurements × 5 flow-cells).

2.3.2. Biofilm composition

2.3.2.1. Inorganic and organic carbon content. The inorganic carbon (IC) and organic carbon (OC) contents of the biofilms grown in exp. 1.1 were measured using an automatic total organic carbon analyser (TOC-V, Shimadzu, Japan). More details about the sample preparation and injection in the analyser can be found for the organic carbon measurement in Derlon et al. (2014). Biofilms of different ages were scratched from the membrane surface using a cell scraper and re-suspended in 50 mL of nanopure water. The biofilm solution was then dispersed for 2 min using an Ultra-Turrax disperser set at power 1 (IKA, Staufen, Germany).

2.3.2.2. Cell and EPS volume. Biofilms grown at 88 and 284 cm water heads and of different ages (7, 14, 21, 28, 35 and 42 d) were analysed in terms of cell and EPS volume. First biofilms on membrane coupons were fixed in a 2% formaldehyde solution for 1 h at 4 °C in the dark. Biofilms were then rinsed with filtered permeate (0.45 µm filtration) and stored in the fridge until analysis. The biofilm structure was examined by confocal laser scanning microscopy (CLSM) using a TCS SP5 (Leica) with an upright microscope controlled by the software LAF AF version 2.7.3.9723. In a preceding experiment the biofilm samples from Chriesbach were subjected to a lectin screening by using all commercially available lectins (72) in order to identify the optimal lectin. For CLSM the fixed biofilm samples from the GDM setup were mounted in a 5 cm Petri dish. Samples were ultimately stained for glycoconjugates by using the lectin IAA from *Iberis amara* (EY laboratories) labelled with Alexa-568 (Molecular Probes). For imaging bacteria, the biofilms were counterstained with Sytox Green (Molecular Probes). CLSM data were recorded using a 25 × NA 0.95 water immersible lens. Around five z-stacks were recorded by sample. Excitation and emission was at 488 nm/495–570 nm (Sytox Green) and 543 nm/580–700 nm (IAA-568). Raw image data was quantified using an extension of the program ImageJ with manual thresholding. Image data sets were projected by employing Imaris ver. 8.1.1 (Bitplane). Relative EPS and cellular volume based on CLSM observations were calculated. Standard deviations were calculated to evaluate the deviation between measurements performed at each time point.

2.3.2.3. Calculations. The relationship between the permeate flux and the TMP is given by Equation (1) (Foley, 2013):

$$J = \frac{\text{TMP}}{\mu \cdot R_{\text{total}}} \quad (1)$$

With the permeate flux J in $\text{m}^3 \text{ m}^{-2} \text{ s}^{-1}$, the TMP in Pa, μ (the dynamic viscosity of water) in Pa s ($1.002 \cdot 10^{-3} \text{ Pa s}$). R_{total} represents the total hydraulic resistance (m^{-1}). The total resistance R_{total} can be represented as the sum of membrane resistance (R_m) and of the cake formed during dead-end filtration (R_{cake}) (Foley, 2013):

$$R_{\text{total}} = R_m + R_{\text{cake}} \quad (2)$$

In our case the cake corresponds to the biofilm formed on the membrane, thus $R_{\text{biofilm}} = R_{\text{cake}}$. During GDM filtration of river water, the resistance due to irreversible fouling is negligible compared to the biofilm resistance. R_{biofilm} indeed represent 95% of the total resistance in the case of biofilms grown with river water during dead-end GDM filtration (Derlon et al., 2012). The irreversible fouling resistance is negligible compared to the biofilm resistance. Also concentration-polarization does not occur during GDM filtration with tolerated biofilm formation on membrane surface. The concentration of polysaccharides and proteins are indeed too low in the feed water (Derlon et al., 2014). Also, these compounds are degraded by bacterial cells (Derlon et al., 2014) and thus do not accumulate on the membrane surface. The resistance of the biofilm can thus be calculated by subtracting the resistance of the membrane to the total resistance derived from the flux and TMP values. R_m was derived from the flux measured when filtering nanopure water through virgin membranes.

The biofilm resistance (m^{-1}) is a function of the specific biofilm resistance α (m kg^{-1}) and of the surface concentration of biofilm ω (kg m^{-2}) (Jorgensen et al., 2012) (Equation (2)):

$$R_{\text{biofilm}} = \alpha \cdot \omega \quad (3)$$

3. Results

3.1. Hydraulic resistances of biofilms grown at constant water heads (exp. 1.1)

The long-term influence of a constant water head on the permeate flux and hydraulic permeability was monitored (Exp.1.1, Fig. 2). Both water heads tested resulted in similar permeate fluxes. For both water head conditions the permeate flux stabilised at around $10 \text{ L m}^{-2} \text{ h}^{-1}$ (Fig. 2, first row). On the contrary, the water head significantly influenced the hydraulic permeability (Fig. 2, second row). Permeability values of around 150 and $50 \text{ L m}^{-2} \text{ h}^{-1} \text{ bar}^{-1}$ were measured at water heads of 88 and 284 cm, respectively. Also, significant variability in the permeate flux/permeability in parallel monitors were noticed between the different biofouling monitors operated at low 88 cm as indicated by the large standard deviations bars (Fig. 2, left-hand column). Such variability between parallel monitors in the permeate flux/permeability were not observed for the biofouling monitors operated at 284 cm water head (Fig. 2, right-hand column).

3.2. Physical structure and composition of the biofilms developed at constant water heads (exp. 1. run 1)

The physical structure and composition of the biofilms developed at constant water heads were monitored. Biofilms developed over long-term at constant water heads of 88 cm or 284 cm had similar mesoscale physical structure (measured ex-situ without TMP, i.e., no permeation) (Fig. 3). Biofilm mean thicknesses increased from 50 to more than 150 µm between day 5 and 42 for both water heads (Fig. 3, top row). The roughness values (absolute and relative) of the different types of biofilms were also similar. For example, the absolute roughness continuously increased from around 15 µm–60 µm between day 5 and 42 for both growth conditions. The mesoscale physical structure of the biofilms developed at 88 cm or 284 cm were thus similar. But one must remember that imaging was performed without any TMP and no permeation forces acting on the biofilms.

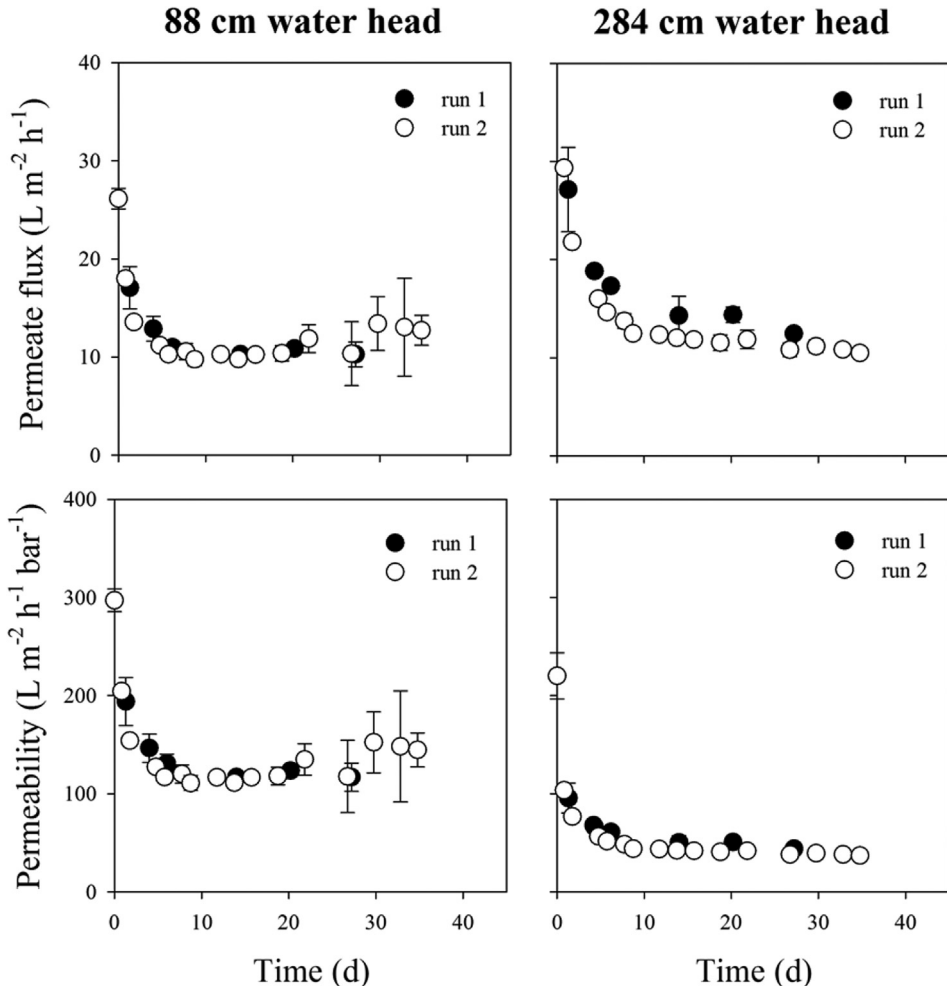


Fig. 2. Change in the permeate flux and in the permeability measured in the GDM systems operated at 88 cm or 284 cm water heads over 45 days (Exp 1.1). Bars indicated the standard variations for the parallel monitors.

Biofilm composition in terms of organic and inorganic carbon surface concentrations (gc m^{-2}) was monitored for biofilms developed at 88 cm water head. Biofilms were mainly composed of inorganic carbon. The ratio of inorganic carbon to total carbon was in average $73 \pm 6\%$ (over the entire filtration period). The TIC and TOC concentrations reached around 0.8 and 0.2 gc m^{-2} at day 43, which corresponds to a biofilm density of $10 \text{ kg}_C \text{ m}^{-3}$ biofilm. However, the density of inorganic carbon components (e.g. calcium carbonate: 2.71 g cm^{-3} or magnesium carbonate: 2.96 g cm^{-3}) significantly exceeds the one of biomass ($10,000 \text{ g m}^{-3}$, i.e., 0.01 g cm^{-3} – here the term biomass refer to cells plus EPS – default value from Henze et al. (1995)). Considering these density values the inorganic carbon components thus represented roughly 1.5% of the biofilm volume after 43 day of growth. The volume of inorganic carbon component is thus negligible compared to the one of organic components such cells and EPS.

A more detailed characterization of the organic fraction of biofilms in terms of EPS and cells was performed. Examples of Z-stack maximum projections monitored for a 14 d old biofilms grown at 88 and 284 cm water heads are shown on Figure SI-2 and SI-3, respectively. CLSM observations indicated the formation of open and heterogeneous biofilm structures. Biofilms were mainly composed of filaments anchored in a biofilm base ("basal layer") and developing towards the bulk liquid. These filaments were colonised by bacteria. Some large particles or aggregates located on

the top of the biofilm basal layer were also observed as well as some cracks and holes.

The relative EPS and cellular volumes were quantified for the different types of biofilms (Fig. 4). Biofilms grown at 88 and 284 cm had similar composition. These biofilms were mainly composed of EPS, with around 90% and 80% of EPS for 43d-old biofilms grown at 88 cm and 284 cm water head, respectively.

3.3. Specific hydraulic resistances of biofilms vs. model cake layer specific resistances

The specific hydraulic resistance of 14 d old biofilms was compared to the one of model cake layers to better understand how the different biofilm fraction (inorganic, organic, cells) influence the biofilm permeability (Fig. 5). The specific hydraulic resistances of the biofilms were significantly higher than those of model cake layers. The 14-day-old biofilms had the highest specific hydraulic resistances ($1.3 \cdot 10^{12} \pm 0.6 \cdot 10^{12} \text{ m kg}^{-1}$). On the other hand model cake layers made of inorganic particles (kaolin, diatoms, etc.) or homogeneous organic particles (such as cells) had the lowest specific hydraulic resistances ($< 5 \cdot 10^{11} \text{ m kg}^{-1}$). The cake layers made of heterogeneous organic matter (i.e., flocs) had an intermediary specific hydraulic resistance ($7.6 \cdot 10^{11} \text{ m kg}^{-1}$).

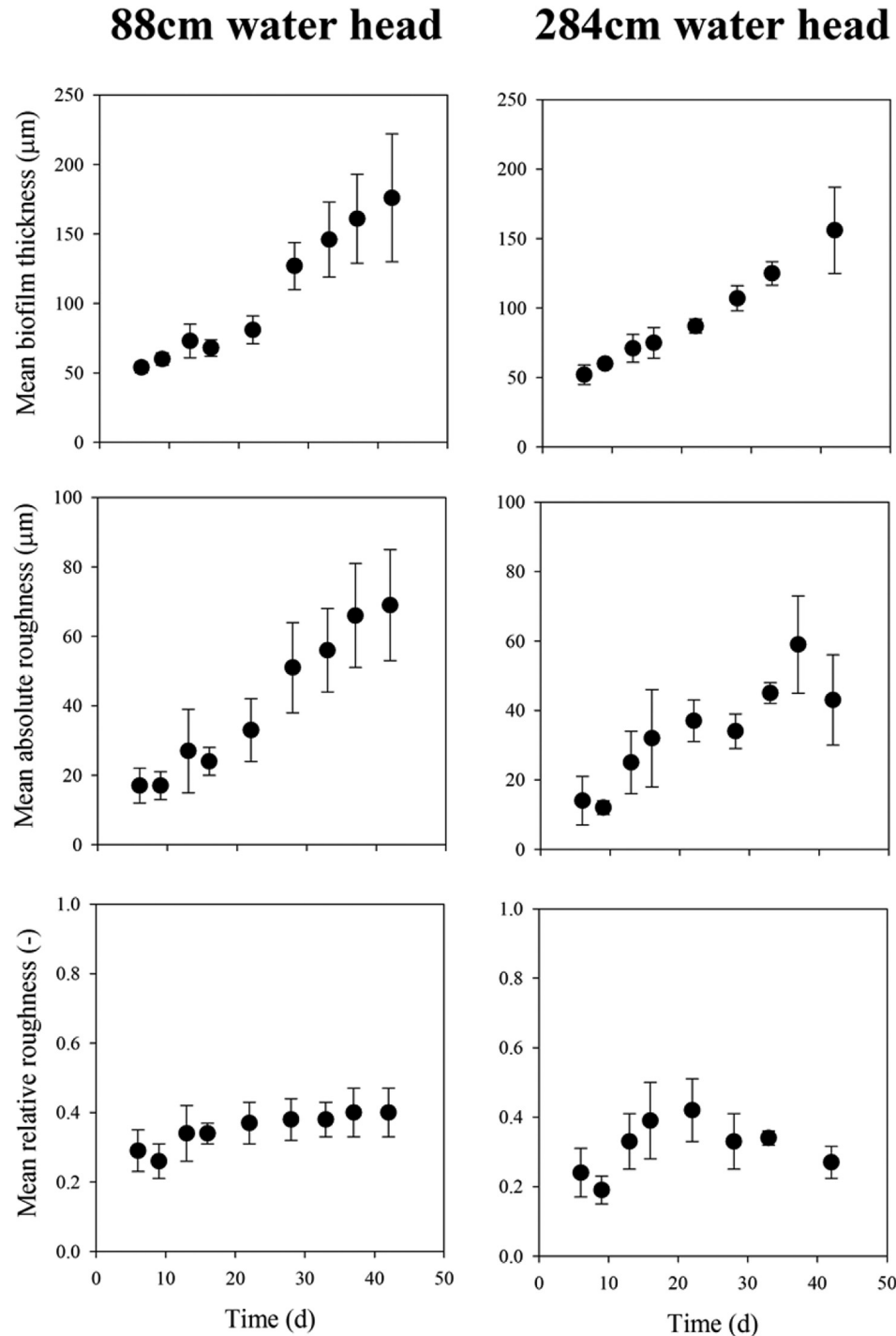


Fig. 3. Influence of the different water heads on the mesoscale physical structure of the biofilms (Exp. 1.1. run 1). Mean biofilm thickness, absolute and relative roughness were monitored over around 50 days. Imaging was performed without TMP, i.e., not under permeation conditions. Bars indicate the standard deviations calculated between measurements.

3.4. Hydraulic resistance of membrane biofilms exposed to a changing TMP (exp. 1.2 and 2)

3.4.1. Effect of a short-term change of TMP

The change in the biofilm resistance (m^{-1}) in response to an increasing TMP was monitored (Fig. 6). The resistance of the biofilm increased almost linearly with an increasing TMP (Fig. 6a). Increasing the TMP from 0.1 to 2.5 bar indeed increased the biofilm resistance from around $4 \cdot 10^{12}$ to $1.6 \cdot 10^{13} \text{ m}^{-1}$. Also, the ageing of

the biofilm did not clearly influence the change in the biofilm hydraulic resistance as a function of the TMP. Biofilm elasticity was evaluated by applying a second TMP step-wise increase (Fig. 6b). The changes in the biofilm hydraulic resistances monitored for the 1st and 2nd TMP step-wise increases were similar.

3.4.2. Effect of a long-term change of water head

The response of the system to a long-term (several days) change of water head was evaluated for biofilms of different ages (5, 16,

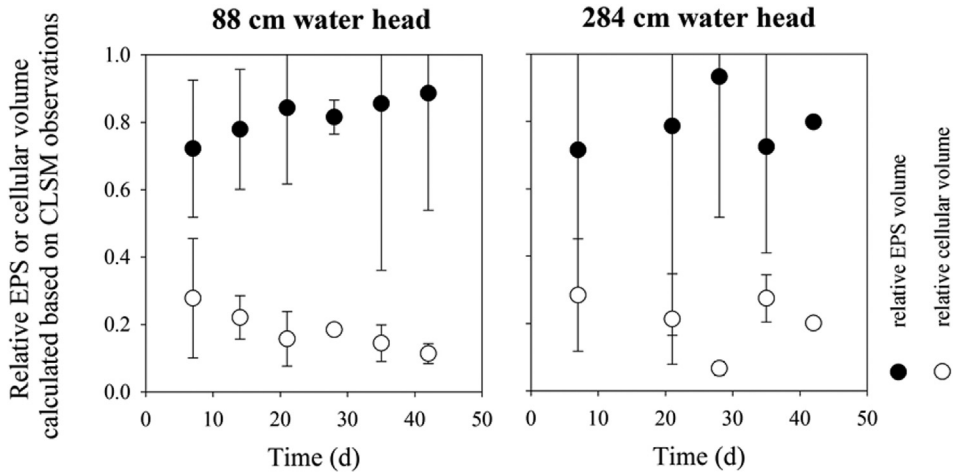


Fig. 4. Change in the relative EPS and cellular volume of EPS calculated from CLSM observations for the two types of biofilms. Bars are shown for each data point and indicate standard deviations between the different Z-stacks monitored with CLSM.

22 d, etc.) that were developed at different initial water heads (exp. 1.2, Fig. 7). A change in the water head triggered a similar response for all biofilms. This response was composed of (i) an immediate change of permeability and (ii) of a time-dependent (long-term) change of permeability. A permeability of around $150 \text{ L m}^{-2} \text{ h}^{-1} \text{ bar}^{-1}$ was measured for a 49-day-old biofilm grown at 88 cm water head (Fig. 7, last graph). Immediately after increasing the water head to 284 cm, the permeability decreased to $100 \text{ L m}^{-2} \text{ h}^{-1} \text{ bar}^{-1}$ (immediate response) and then continued decreasing for around 10 d to ultimately reach a constant value of $60 \text{ L m}^{-2} \text{ h}^{-1} \text{ bar}^{-1}$ (time-dependent response).

4. Discussion

4.1. Biofilm composition determines its hydraulic permeability

Our results demonstrate that the specific hydraulic resistances of biofilms developed on membrane surfaces during dead-end

ultrafiltration significantly exceed those of model cake layers made of inorganic or organic particles (Fig. 5). A main question is therefore to discuss the respective influence of the different biofilm fractions (inorganic materials, cells, EPS) on its permeability.

The biofilms tested in our study were mainly composed of inorganic carbon component (more than 70% in mass). But inorganic carbon components represented however a negligible fraction of the biofilm volume due to their high density (roughly 1.5% of the biofilm volume after 43 days of growth). We compared the specific hydraulic resistances of biofilms to the ones of model cake layers made of inorganic particles (Fig. 5). Model cake layers of inorganic particles alone had very low specific hydraulic resistance compared to biofilm hydraulic resistances. Similar observations regarding the low hydraulic resistances of inorganic particles were reported for cake layers (Tiller and Kwon, 1998) or biofilms on membranes (Chomiak et al., 2014). Chomiak et al. (2014) compared the hydraulic resistance of control biofilms to the ones of biofilms supplemented with kaolin or diatoms. The control biofilms had much lower mass and thickness than biofilms supplemented with inorganic particles. However, its specific resistance was much higher (Chomiak et al., 2014). Chomiak et al. (2014) noticed that inorganic particles promote the formation of porous biofilms structures associated with a low overall hydraulic resistance. We can thus claim that the high resistance of biofilms likely does not result from the presence of inorganic carbon components in its structure.

The organic fraction of biofilms represented a low fraction of the biofilm mass (around 30%) but the main fraction of the biofilm volume (roughly 98.5% for a 43-day-old biofilm). The organic fraction of biofilms consisted mainly of bacterial cells embedded in the EPS matrix. The cell volume accounted for a minor fraction of the biofilm volume. But the hydraulic resistance of model cake layers made of bacterial cells was significantly lower than the one of biofilms (Fig. 5). This suggests that bacterial cells have no or very little influence on the biofilm hydraulic resistance, similarly to inorganic carbon components. Dreszer et al. (2013) previously reported about the negligible influence of cells on the biofilm hydraulic resistance.

The EPS matrix is the glue that holds the cells and other particles together. In our study, EPS glycoconjugates accounted for more than 90% of the biofilm volume (for a 43d-old biofilm grown at 88 cm water head). If cells and inorganic particles have a negligible impact on the hydraulic resistance, then the EPS matrix might be the main fraction determining the biofilm permeability. In our

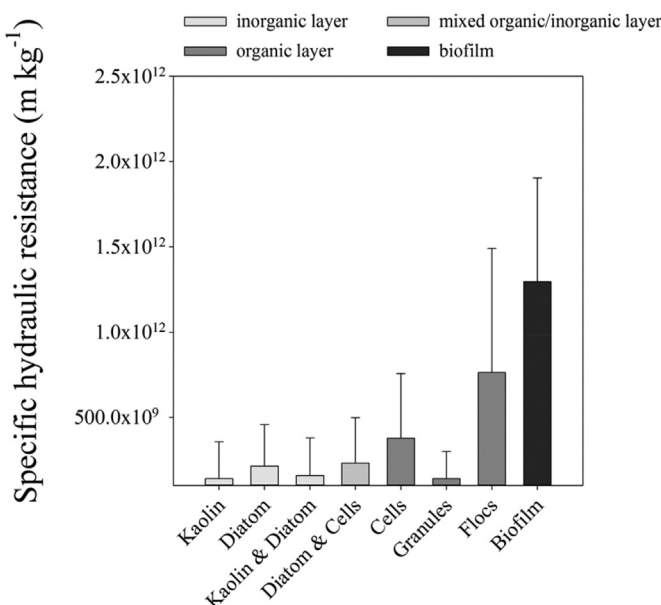


Fig. 5. Specific hydraulic resistance of biofilms vs. of model cake layers (i.e., kaolin, diatom, etc.).

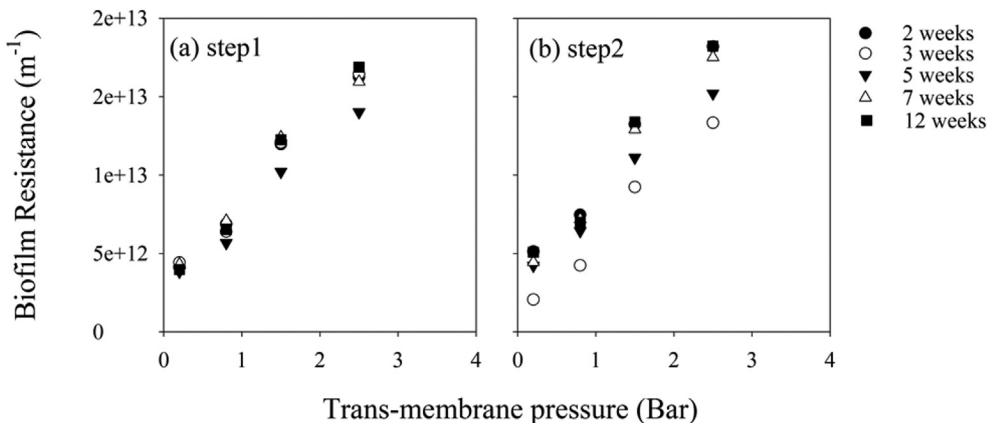


Fig. 6. Changes in the biofilm resistance (m^{-1}) in response to an increasing TMP (bar). For each biofilm, two compressibility tests were performed with 4 min relaxation time in between.

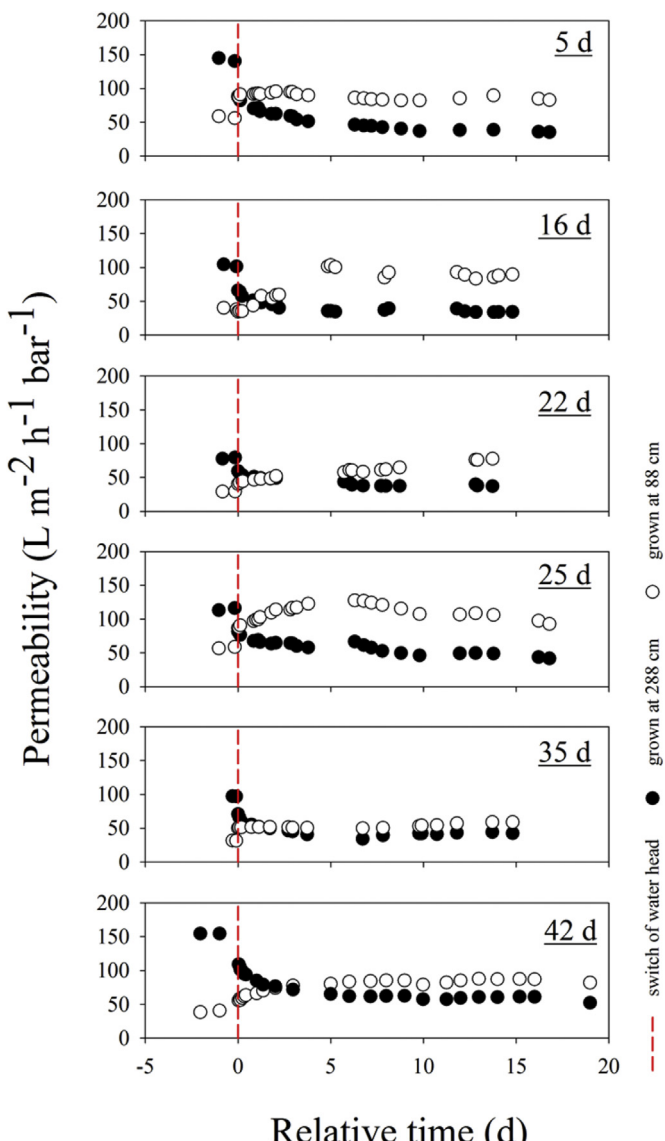


Fig. 7. Influence of a long-term change of water head on the permeability of biofilms of different ages (Exp 1.2.).

study, the higher hydraulic resistances were always observed for materials that contained a significant fraction of EPS (bacterial flocs, granules, biofilms). Stewart (2012) also proposed that the predominant resistance to flow in a microbial aggregate is posed by extracellular matrix material. The effect of EPS can be (i) detrimental, i.e., by increasing the friction forces at the scale of EPS matrix network or (ii) beneficial, i.e., by engineering an internal biofilm architecture that is more/less permeable due to the presence of voids/channels. In the case of polymer gels, the water flowing through the gel experiences hydrodynamic friction from the polymer network (Suzuki et al., 2009). Friction is the force that resists to the movement of a fluid along the surface of a material. We can hypothesize that the permeation rate through the biofilm EPS matrix results from similar mechanisms, i.e., the balance between the resistive forces (friction) and the forces that drive the water through the biofilms. The pore size, heterogeneity and spatial arrangement of the EPS matrix determines the permeability of model biofilms (Billings et al., 2015). But the degree of organization of the EPS matrix, as random arrangements or specifically linked constituents, remains to be established (Neu and Lawrence, 2015). Also the EPS matrix determines the overall internal structure of the biofilm, i.e., the presence of voids or channels. The presence of voids/channels can be beneficial to permeation as it can result in preferential pass through the biofilm.

In conclusion, our study provides relevant insights about the link between the biofilm composition and its hydraulic resistance. We demonstrated that inorganics and cells represented a minor fraction of the biofilm volume and that they have a limited influence on the overall biofilm hydraulic resistance. On the other hand, our results indicate that EPS has the greater impact on the biofilm hydraulic resistance.

4.2. Biofilms are compressible structures

Another main finding of our study is that biofilms are highly compressible structures (Figs. 6 and 7). The response of biofilms to a change of TMP has two components: (i) an immediate response and (ii) a long-term response (over few days or weeks).

A sudden change of TMP triggers an immediate relaxation/compression of the biofilms, and ultimately a change in the biofilm hydraulic resistance (Figs. 6 and 7). The relaxation/compression of the biofilms directly determined its physical structure. Biofilms grown at two different TMPs have similar physical properties when then imaged a similar TMP using OCT (Fig. 3). The biofilm resistance increased proportionally to the TMP as a result of the biofilm

compression. Similarly to concentration polarization models (Cheryan and Cheryan, 1998), the linear correlation between the biofilm resistance and TMP suggests that biofilm resistance is a function of the permeability of the biofilm and of its thickness (i.e. the travel distance of the water). The TMP determines the forces acting on the biofilms and in turn its internal biofilm organization, i.e., its packing. Applying a physical stress deforms the biofilm structure and changes the void space, thus reducing its porosity (Laspidou et al., 2014). The composition of biofilms likely governs its mechanical stability, i.e., to what extent the biofilm resists to the compression forces. Dreszer et al. (2014) proposed that two mechanisms govern the biofilm compressibility: a physical compression of the EPS and a chemical EPS consolidation. However in our study, similar hydraulic resistances were measured for the 1st and 2nd compressibility tests, indicating that in our test the compression of the biofilms was entirely reversible. These results are in accordance with the study of Vallares Linares et al. (2016), who reported that the effect of permeate flux on the hydraulic biofilm resistance is reversible (Vallares Linares et al., 2016). Our results also suggest that chemical EPS consolidation did not occur during the 1st compression test and did not modify the mechanical properties of the biofilms submitted to the 2nd test. The elasticity of biofilms also explains why similar mesoscale physical structures were observed without TMP for the two types of biofilm (Fig. 3). The key role of polymeric substances in determining the compressibility of cake layers formed in membrane bioreactors was also reported (Poorasgari et al., 2015). Both cake layers formed during the filtration of activated sludge and gel layers formed during filtration of soluble microbial products were shown to be compressible (Poorasgari et al., 2015). However, the biofilms tested in our study do not behave exactly as gel layers made of EPS. Gel layers made of EPS are indeed not compressible at low TMP and a compressibility yield stress must be exceeded to observe compression of the gel. An opposite behavior is observed with biofilms, as biofilms compress as soon as a small TMP is applied (Fig. 6). This comparison suggests that the mechanical properties of biofilms and gel layers made of EPS are different, even though those two structures are compressible.

We also evaluated how the biofilms respond to a long-term change of TMP (Fig. 7). A long-term change of the water heads resulted in (i) an immediate change of the biofilm hydraulic resistance followed by (ii) an additional long-term variation (Fig. 7). Different mechanisms govern these immediate and long-term variations of hydraulic resistance. It is proposed that the immediate response of the biofilm to a TMP change is governed by its mechanical properties (e.g. elasticity), while its long-term response results from different mechanisms. It is unclear what exact mechanism lies behind this long-term variation of the biofilm hydraulic resistance. We hypothesized that the internal biofilm architecture re-organizes, i.e., a new self-arrangement of the internal biofilm structure occurs and ultimately modify the biofilm hydraulic resistance. However, it remains unclear if this long-term variation of biofilm hydraulic resistance results from physical, chemical or microbial mechanisms. But this suggests that the history/memory of the biofilms also influence its hydraulic resistance.

4.3. Practical implications

Biofouling occurs in all membrane systems and reduces the permeate flux. The TMP is usually increased to maintain the system performances, i.e., a constant permeate flux. But our results clearly demonstrate that biofilms respond immediately and then adapt to TMP rises. Thus, maintaining constant flux requires larger TMP rise due to the compression of the biofilms. Such effect can be expected in all membrane systems where biofilm formation represents the

dominant fouling mechanism. A new strategy to operate membrane systems relies on taking advantages of the biofilm that inevitably grows on membrane surfaces. For these biofilm + membrane composite systems, increasing the production of clean water requires increasing the membrane surface and cannot be achieved through increasing the water head.

5. Conclusions

The main conclusions of this study are:

- Biofilms are highly compressible structures. As a consequence, increasing TMP results in an increased biofilm hydraulic resistance. The response of the biofilm to a pressure change has two components: (i) an instantaneous response due to the compression/relaxation of the existing biofilm structure and (ii) a long-term response due to the self re-organization of the internal biofilm architecture.
- The hydraulic resistance of membrane biofilms results from three parameters: the biofilm composition, the instantaneous forces acting on the biofilm structure, and the biofilm growth history.
- Biofilm composition (in terms of biofilm volume) is dominated by EPS glycoconjugates and the EPS fraction determined the biofilm hydraulic resistance. Bacteria and inorganic particles provided very little to no resistance to permeation.

Appendix A. Supplementary data

Supplementary data related to this article can be found at <http://dx.doi.org/10.1016/j.watres.2016.06.019>.

References

- Billings, N., Birjiniuk, A., Samad, T.S., Doyle, P.S., Ribbeck, K., 2015. Material properties of biofilms – a review of methods for understanding permeability and mechanics. *Rep. Prog. Phys.* 78 (3).
- Cheryan, M., Cheryan, M., 1998. Ultrafiltration and Microfiltration Handbook. Pa., Technomic Pub. Co, Lancaster.
- Chomiak, A., Sinnen, B., Derlon, N., Morgenroth, E., 2014. Inorganic particles increase biofilm heterogeneity and enhance permeate flux. *Water Res.* 64, 177–186.
- de Beer, D., Stoodley, P., Lewandowski, Z., 1994. Liquid flow in heterogeneous biofilms. *Biotechnol. Bioeng.* 44 (5), 636–641.
- de Beer, D., Stoodley, P., Lewandowski, Z., 1996. Liquid flow and mass transport in heterogeneous biofilms. *Water Res.* 30 (11), 2761–2765.
- Derlon, N., Koch, N., Eugster, B., Posch, T., Pernthaler, J., Pronk, W., Morgenroth, E., 2013. Activity of metazoa governs biofilm structure formation and enhances permeate flux during Gravity-Driven Membrane (GDM) filtration. *Water Res.* 47 (6), 2085–2095.
- Derlon, N., Mimoso, J., Klein, T., Koetzsch, S., Morgenroth, E., 2014. Presence of biofilms on ultrafiltration membrane surfaces increases the quality of permeate produced during ultra-low pressure gravity-driven membrane filtration. *Water Res.* 60, 164–173.
- Derlon, N., Peter-Varbanets, M., Scheidegger, A., Pronk, W., Morgenroth, E., 2012. Predation influences the structure of biofilm developed on ultrafiltration membranes. *Water Res.* 46 (10), 3323–3333.
- Dreszer, C., Vrouwenvelder, J.S., Paulitsch-Fuchs, A.H., Zwijnenburg, A., Kruithof, J.C., Flemming, H.C., 2013. Hydraulic resistance of biofilms. *J. Membr. Sci.* 429, 436–447.
- Dreszer, C., Wexler, A.D., Drusova, S., Overdijk, T., Zwijnenburg, A., Flemming, H.C., Kruithof, J.C., Vrouwenvelder, J.S., 2014. In-situ biofilm characterization in membrane systems using optical coherence tomography: formation, structure, detachment and impact of flux change. *Water Res.* 67, 243–254.
- Flemming, H.-C., Szewzyk, U., Griebe, T., 2000. Biofilms: Investigative Methods & Applications. Technomic Publishing Co, Lancaster, Pa.
- Foley, G., 2013. Membrane Filtration. Cambridge University Press.
- Henze, M., Harremoës, P., Jansen, J.L.C., Arvin, E., 1995. Wastewater Treatment: Biological and Chemical Processes. Springer Edt., Berlin.
- Jorgensen, M.K., Bugge, T.V., Christensen, M.L., Keiding, K., 2012. Modeling approach to determine cake buildup and compression in a high-shear membrane bioreactor. *J. Membr. Sci.* 409, 335–345.
- Laspidou, C.S., Spyrou, L.A., Aravas, N., Rittmann, B.E., 2014. Material modeling of biofilm mechanical properties. *Math. Biosci.* 251 (0), 11–15.
- Lewandowski, Z., Stoodley, P., Altobelli, S., 1995. Experimental and conceptual

- studies on mass transport in biofilms. *Water Sci. Technol.* 31 (1), 153–162.
- McDonogh, R., Schaule, G., Flemming, H.C., 1994. The permeability of biofouling layers on membranes. *J. Membr. Sci.* 87 (1–2), 199–217.
- Neu, T.R., Lawrence, J.R., 2015. Innovative techniques, sensors, and approaches for imaging biofilms at different scales. *Trends Microbiol.* 23 (4), 233–242.
- Poorasgari, E., Bugge, T.V., Christensen, M.L., Jorgensen, M.K., 2015. Compressibility of fouling layers in membrane bioreactors. *J. Membr. Sci.* 475, 65–70.
- Smith, A.L., Skerlos, S.J., Raskin, L., 2015. Membrane biofilm development improves COD removal in anaerobic membrane bioreactor wastewater treatment. *Microb. Biotechnol.* 8 (5), 883–894.
- Stewart, P.S., 2012. Mini-review: convection around biofilms. *Biofouling* 28 (2), 187–198.
- Stoodley, P., de Beer, D., Lewandowski, Z., 1994. Liquid flow in biofilm systems. *Appl. Environ. Microbiol.* 60 (8), 2711–2716.
- Stoodley, P., Lewandowski, Z., Boyle, J.D., Lappin-Scott, H.M., 1999a. Structural deformation of bacterial biofilms caused by short-term fluctuations in fluid shear: an in situ investigation of biofilm rheology. *Biotechnol. Bioeng.* 65 (1), 83–92.
- Stoodley, P., Lewandowski, Z., Boyle, J.D., Lappin-Scott, H.M., 1999b. The formation of migratory ripples in a mixed species bacterial biofilm growing in turbulent flow. *Environ. Microbiol.* 1 (5), 447–455.
- Suzuki, Y.Y., Tokita, M., Mukai, S., 2009. Kinetics of water flow through a polymer gel. *Eur. Phys. J. E* 29 (4), 415–422.
- Tiller, F.M., Kwon, J.H., 1998. Role of porosity in filtration: XIII. Behavior of highly compactible cakes. *Aiche J.* 44 (10), 2159–2167.
- Vallares Linares, R., Wexler, A.D., Bucs, S.S., Dreszer, C., Zwijnenburg, A., Flemming, H.C., Kruithof, J.C., Vrouwenvelder, J.S., 2016. Compaction and relaxation of biofilms. *Desalination Water Treat.* 57 (28), 12902–12914.
- Vinogradov, E., Sadovskaya, I., Li, J.J., Jabbouri, S., 2006. Structural elucidation of the extracellular and cell-wall teichoic acids of *Staphylococcus aureus* MN8m, a biofilm forming strain. *Carbohydr. Res.* 341 (6), 738–743.